Title

Cellular responses to reactive oxygen species are predicted from molecular mechanisms

Journal

Proceedings of the National Academy of Sciences of the United States of America, 116(28)

ISSN

0027-8424

Authors

Yang, Laurence
Mih, Nathan
Anand, Amitesh
et al.

Publication Date

2019-07-09

DOI

10.1073/pnas.1905039116

Peer reviewed

Cellular responses to reactive oxygen species are predicted from molecular mechanisms

Laurence Yang[a,1,2], Nathan Mih[b,c], Amitesh Anand[a], Joon Ho Park[b], Justin Tan[a], James T. Yurkovich[a,c,3], Jonathan M. Monk[a], Colton J. Lloyd[a], Troy E. Sandberg[a], Sang Woo Seo[a,4], Donghyuk Kim[a,5], Anand V. Sastry[a], Patrick Phaneuf[c], Ye Gao[d], Jared T. Broddrick[d], Ke Chen[a], David Heckmann[a], Richard Szubin[a], Ying Hefner[a], Adam M. Feist[a,e], and Bernhard O. Palsson[a,e,f,1]

[a]Department of Bioengineering, University of California San Diego, La Jolla, CA 92093; [b]Department of Nanoengineering, University of California San Diego, La Jolla, CA 92093; [c]Bioinformatics and Systems Biology Program, University of California San Diego, La Jolla, CA 92093; [d]Division of Biological Sciences, University of California San Diego, La Jolla, CA 92093; [e]The Novo Nordisk Foundation Center for Biosustainability, Technical University of Denmark, 2800 Kongens Lyngby, Denmark; and [f]Department of Pediatrics, University of California San Diego, La Jolla, CA 92093

Edited by James E. Cleaver, University of California, San Francisco, CA, and approved June 3, 2019 (received for review March 25, 2019)

Catalysis using iron–sulfur clusters and transition metals can be traced back to the last universal common ancestor. The damage to metalloproteins caused by reactive oxygen species (ROS) can prevent cell growth and survival when unmanaged, thus eliciting an essential stress response that is universal and fundamental in biology. Here we develop a computable multiscale description of the ROS stress response in *Escherichia coli*, called OxidizeME. We use OxidizeME to explain four key responses to oxidative stress: 1) ROS-induced auxotrophy for branched-chain, aromatic, and sulfurous amino acids; 2) nutrient-dependent sensitivity of growth rate to ROS; 3) ROS-specific differential gene expression separate from global growth-associated differential expression; and 4) coordinated expression of iron–sulfur cluster (ISC) and sulfur assimilation (SUF) systems for iron–sulfur cluster biosynthesis. These results show that we can now develop fundamental and quantitative genotype–phenotype relationships for stress responses on a genome-wide basis.

reactive oxygen species | oxidative stress | metabolism | protein expression | genome-scale model

Aerobic organisms have evolved cellular responses to oxidative stress over 3 billion years since oxygenation of the Earth's atmosphere (1). Oxygen toxicity is manifested in damage to cellular components by reactive oxygen species (ROS), which are generated as a by-product of maintaining an aerobic lifestyle (2, 3). Specifically, cells generate ROS when flavin, quinol, or iron cofactors are autoxidized (2). ROS damage DNA, certain iron-containing metalloproteins, and other cellular processes (4). In addition to endogenously produced ROS, microbes are exposed to exogenous sources of ROS in the form of H_2O_2, superoxide, or redox-cycling compounds that eukaryotes or other microbes generate as a means of inflicting oxidative stress on competitors (5, 6). For example, the human immune system employs macrophages that use ROS to combat pathogens. While most microbes are weakened by this oxidative stress, certain pathogens can grow inside the phagosome (7).

Overall, microbes combat oxidative stress by reducing ROS generation, increasing ROS detoxification capacity, and protecting or repairing the targets of ROS that include metabolites and macromolecules. Enzymes adapted against oxidative stress have developed tolerance mechanisms that include shielding vulnerable metal centers by accessory domains, evolving of iron cofactors into less oxidizable forms, and replacement of iron with alternative metal ions. (8).

Despite the fundamental importance of ROS damage on cellular functions, we lack a framework that connects known and hypothesized individual molecular targets of ROS to systemic physiological responses. Here, we address this gap using a genome-scale computational systems biology approach focused on the processes that determine homeostasis of iron, which is essential for *Eschericia coli*'s growth, yet is vulnerable to ROS.

Results

Model Construction. Herein we describe the reconstruction of our computable multiscale description of ROS damage to metalloproteins. Here, multiscale means that we model reactions involved in the processes of protein expression (slow) and metabolism (fast), as described previously (9). These rates can span 15 orders of magnitude, so we use specialized (quad-precision) solvers to compute steady-state solutions (10). We

Significance

All aerobic life requires management of reactive oxygen species (ROS), which damage cellular components. Cells generate ROS endogenously when flavin, quinol, or iron cofactors are autoxidized. ROS damage DNA, certain iron metalloproteins, and other cellular processes. In addition to inherent endogenous ROS production, eukaryotes and microbes produce exogenous ROS as H_2O_2, superoxide, or redox-cycling compounds to inflict oxidative stress on competitors. Despite the fundamental impact of ROS damage on cellular functions, a framework that connects known and hypothesized individual molecular targets of ROS to systemic physiological responses is lacking. We address this gap by reconstructing a genome-scale model and using it to compute *E. coli*'s systems-level balancing between iron homeostasis and ROS management.

Author contributions: L.Y. and B.O.P. designed research; L.Y., N.M., A.A., J.H.P., J.T., J.T.Y., J.M.M., C.J.L., T.E.S., S.W.S., D.K., A.V.S., P.P., Y.G., J.T.B., K.C., D.H., R.S., Y.H., and A.M.F. performed research; L.Y., N.M., A.A., J.H.P., J.T., and T.E.S. analyzed data; and L.Y., N.M., and B.O.P. wrote the paper.

The authors declare no conflict of interest.

This article is a PNAS Direct Submission.

Data deposition: Code has been deposited on GitHub (https://github.com/SBRG/oxidizeme), and data for evolved strains have been deposited in ALEdb, https://aledb.org (Project ID OxidizeME).

[1]To whom correspondence may be addressed. Email: lyang@eng.ucsd.edu or palsson@ucsd.edu.

[2]Present address: Department of Chemical Engineering, Queen's University, Kingston, ON K7L 3N6, Canada.

[3]Present address: Institute for Systems Biology, Seattle, WA 98109.

[4]Present address: School of Chemical and Biological Engineering, Seoul National University, Seoul 08826, Republic of Korea.

[5]Present address: School of Energy and Chemical Engineering, Ulsan National Institute of Science and Technology, Ulsan 44919, Republic of Korea.

This article contains supporting information online at www.pnas.org/lookup/suppl/doi:10.1073/pnas.1905039116/-/DCSupplemental.

Published online July 3, 2019.

begin with a published reconstruction of *E. coli*'s integrated metabolic and macromolecular expression (ME) networks (11). This ME model accounts for 1,678 genes, 7,031 metabolites, and 12,655 reactions. The model includes detailed pathway reconstruction for transcription, translation, complex formation, and prosthetic group engraftment (12–14). The model also maps protein complex–metal stoichiometries, including 43 complexes that incorporate mononuclear iron or iron–sulfur clusters. We reconstruct ROS-based damage and cellular repair processes for these metalloproteins, yielding the OxidizeME model (Fig. 1) as described below.

First, we define mathematical expressions to quantitatively describe the damage of iron–sulfur (Fe–S) clusters by superoxide and H_2O_2. The net reactions for Fe–S cluster damage are (4)

$$[\text{4Fe-4S}]^{2+} + O_2^{\cdot-} + 2\,H^+ \rightarrow [\text{3Fe-4S}]^{1+} + Fe^{2+} + H_2O_2,$$
$$[\text{4Fe-4S}]^{2+} + H_2O_2 + 2\,H^+ \rightarrow [\text{3Fe-4S}]^{1+} + Fe^{3+} + 2\,H_2O.$$

Assuming that the ROS concentration $[ROS] \ll K_M$, the rate of Fe–S cluster damage v^{dmg} depends on $[ROS]$, the rate constant $(k_{cat}/K_M)^{dmg}$, and the Fe–S protein concentration E,

$$v^{dmg} = \left(\frac{k_{cat}}{K_M}\right)^{dmg}[ROS]\cdot E = \left(\frac{k_{cat}}{K_M}\right)^{dmg}[ROS]\cdot v^{dil}/\mu, \quad [1]$$

where μ is the cell's specific growth rate in h^{-1} and v^{dil} is the dilution rate of the protein.

Second, we describe Fe–S cluster repair. We assume that *yggX* (15) or *ytfE* (16) repairs Fe–S clusters using NADH as the electron donor and define the net repair reaction:

$$[\text{3Fe-4S}]^{1+} + Fe^{2+} + \text{NADH} \rightarrow [\text{4Fe-4S}]^{2+} + \text{NAD}^+.$$

The repair rate v^{repair} is constrained by the concentrations of the set of repair proteins $\mathcal{R} = \{\text{YggX, YtfE}\}$ and their rate constants of Fe–S cluster repair k_{repair}:

$$v^{repair} \le \sum_{j\in\mathcal{R}} k_{repair,j}\cdot E_j = \sum_{j\in\mathcal{R}} k_{repair,j}\cdot v_j^{dil}/\mu. \quad [2]$$

Third, we describe the demetallation and mismetallation of mononuclear iron metalloproteins. Assuming $[ROS] \ll K_M$, the demetallation rate of protein j by the ROS $k \in \mathcal{O} = \{O_2^{\cdot-}, H_2O_2\}$ is defined as

$$v_{jk}^{demet} = k_{jk}^{demet}[ROS]v_j^{dil}/\mu, \quad [3]$$

where k_{jk}^{demet} is the demetallation rate constant. Next, to describe mismetallation by competing metals, we assume that metallation occurs rapidly and is close to equilibrium (17). We use the metal–protein stability constant of metal i (β_j^i) relative to β_j^{Fe}, along with relative metal concentrations ([Metal i]/[Fe(II)]). We then define the rate that protein j is metallated with metal i as

$$v_j^{metal,i} = \frac{\beta_j^i[\text{Metal } i]}{\beta_j^{Fe}[\text{Fe(II)}]}\left(\sum_{k\in\mathcal{O}}\left(v_{jk}^{demet}\right) + v_j^{dil}\right). \quad [4]$$

We consider the set of alternative metals $\mathcal{M} = \{\text{Mn(II), Co(II), Zn(II)}\}$. We then scale the catalytic efficiency k_{eff} of the alternatively metallated enzymes based on estimates from published data (18, 19).

Finally, we formulate an optimization problem to compute the metabolic and proteomic state of *E. coli* under ROS stress. In the original ME model, the flux state (v)—for metabolic and macromolecular expression reactions—that maximizes growth rate is computed by solving the problem (10, 11)

$$\max_{\mu,v}\ \mu \text{ subject to } S(\mu)\cdot v = 0,\ l \le v \le u, \quad [5]$$

where $S(\mu)$ is a stoichiometric matrix that includes coefficients that depend on μ, and l, u are lower and upper flux bounds. In OxidizeME, the corresponding problem is the following:

$$\begin{aligned}
\max_{\mu,v}\quad & \mu \\
\text{subject to}\quad & S(\mu)\cdot v = 0, \\
& l \le v \le u, \\
& v_j^{dmg} - v_j^{repair} - v_j^{dil} = 0,\ \forall j \in \mathcal{D}, \\
& v_j^{dmg} = \left(\frac{k_{cat}}{K_M}\right)_j^{dmg}[ROS]v_j^{dil}/\mu,\ \forall j \in \mathcal{D}, \\
& v_j^{dil} \ge \sum_{i\in\mathcal{R}} \frac{\mu}{k_{repair\,i}} v_{ij}^{repair},\ \forall j \in \mathcal{D}, \\
& \sum_{j\in\mathcal{D}} v_{ij}^{repair} \le \sum_{i\in\mathcal{R}} k_{repair,i}\cdot v_i^{dil}/\mu, \\
& v_{jk}^{demet} = k_{jk}^{demet}[ROS]v_j^{dil}/\mu, \\
& v_j^{metal,i} = \frac{\beta_j^i[\text{Metal } i]}{\beta_j^{Fe}[\text{Fe(II)}]}\left(\sum_{k\in\mathcal{O}}\left(v_{jk}^{demet}\right) + v_j^{dil}\right), \\
& \forall i \in \mathcal{M}, \forall j \in \mathcal{D}. \quad [6]
\end{aligned}$$

Comparing simulations with measured proteomics (20), we find that OxidizeME computes up to 85% of the *E. coli* proteome by mass (Dataset S1). Code and documentation for OxidizeME are available at https://github.com/SBRG/oxidizeme.

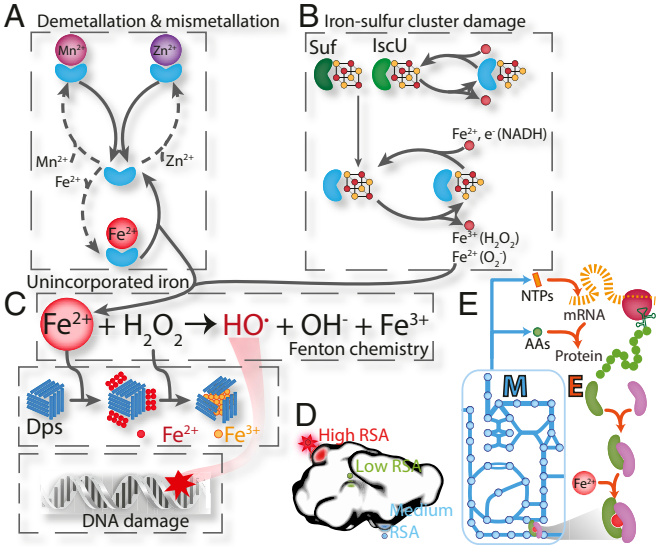

Fig. 1. OxidizeME: a multiscale description of metabolism and macromolecular expression that accounts for damage by ROS to macromolecules. (*A*) Mononuclear Fe(II) proteins are demetallated by ROS and mismetallated with alternative divalent metal ions. (*B*) Iron–sulfur clusters are oxidized and repaired. (*C*) Unincorporated Fe(II) spontaneously reacts with H_2O2 via Fenton chemistry, generating hydroxyl radicals that damage DNA, while the Dps protein stores unincorporated iron and protects DNA from damage. (*D*) Protein structural properties are computed to estimate the probability of metal cofactor damage by ROS (RSA: relative solvent accessibility). (*E*) Processes in *A*–*D* are integrated into a multiscale oxidative model, named OxidizeME. OxidizeME is used to compute the scope of macromolecular damage and the cellular response for varying intracellular concentrations of superoxide, hydrogen peroxide, and divalent metal ions (Fe(II), Mn(II), Co(II), Zn(II)); see *SI Appendix* for details.

Amino Acid Auxotrophy under Oxidative Stress. A hallmark response to ROS damage for *E. coli* is the deactivation of branched-chain and aromatic amino acid biosynthesis pathways, which is alleviated by supplementing these amino acids (4). Compared with supplementing all 20 amino acids, OxidizeME correctly predicted that excluding Ile and Val had a greater impact on growth rate than did excluding Phe, Trp, and Tyr (Fig. 2*A*). The reason that *E. coli* cannot grow under ROS stress without supplementation of branched-chain amino acids is that the iron–sulfur clusters of dihydroxy-acid dehydratase and isopropylmalate isomerase are inactivated by ROS, thus debilitating the branched-chain amino acid biosynthetic pathway (21). The auxotrophy for aromatic amino acids was originally attributed to inactivation of the transketolase reaction (22), but was recently traced to the mismetallation of the mononuclear iron cofactor in 3-deoxy-D-arabinheptulosonate 7-phosphate (DAHP) synthase (19). OxidizeME correctly predicted these molecular mechanisms and their phenotypic consequences (Fig. 2).

Meanwhile, the basis of sulfurous amino acid auxotrophy in *E. coli* remains inconclusive despite multiple investigations (23, 24). OxidizeME correctly predicted auxotrophy for sulfurous amino acids (cysteine and methionine) under ROS stress (Fig. 2*A*). We traced a plausible mechanism to damage of the iron–sulfur cluster in CysI, which catalyzes the sulfite reductase step of Cys biosynthesis. Sulfite reductase binds four cofactors: iron–sulfur, FAD, FMN, and siroheme. Consistent with prior studies (25), our structural model estimated the siroheme group of sulfite reductase to be difficult to reach by ROS, mainly due to the depth of the cofactor binding residue (Dataset S2). Previous studies showed that the iron–sulfur cluster is likely not autoxidized with molecular oxygen because it is not solvent exposed (25). However, our structural model predicted that the iron–sulfur cluster is reached by ROS when considering both solvent exposure and depth of the cluster-binding residue from the solvent-accessible surface (Dataset S2). Simulations confirmed that alleviating damage to sulfite reductase was sufficient to reverse the observed growth rate defect and enable growth at higher ROS concentrations in the absence of Cys and Met (Fig. 2 *B* and *C*). Our hypothesis that sulfite reductase is deactivated by ROS is consistent with studies in *Salmonella enterica* showing that the activity of this enzyme is indeed reduced by elevated superoxide (26). Furthermore, the deactivation of sulfite reductase is consistent with accumulation of its substrate, sulfite, and explains the previously observed accumulation of sulfite (24). We note that CysI inactivation does not exclude the possibility that superoxide additionally leads to cell envelope damage, facilitating leakage of small molecules (27). Thus, OxidizeME can be used to understand and predict the basis for amino acid auxotrophies as a systemic response to specific macromolecular vulnerabilities to ROS.

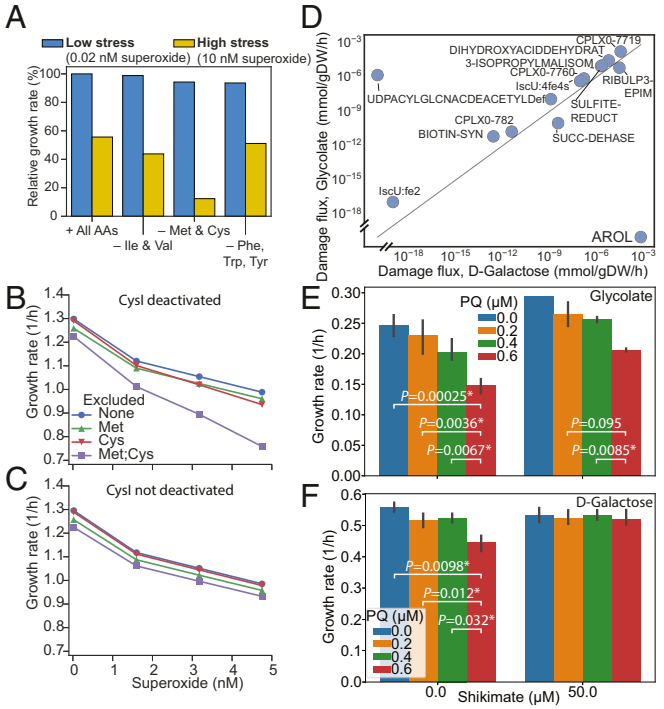

Fig. 2. Systemic consequences of ROS stress. (*A*) Predicted optimal growth rate under low and high superoxide concentrations with different supplementation of amino acids (AAs). "All AAs" refers to all 20 common amino acids, and "–Ile & Val" means all amino acids except Ile and Val were supplemented. (*B*) Predicted optimal growth rate vs. superoxide concentration in various sulfurous amino acid supplementation media. (*C*) Same as *B* but simulated without damage to CysI by ROS. (*D*) Simulated damage fluxes for growth on glycolate vs. D-galactose. AROL: shikimate kinase II. (*E*) Growth rate of MG1655 on glycolate minimal medium with 0 to 0.6 μM PQ, with and without 50 μM shikimate supplementation. (*F*) Same as *E* but for growth on D-galactose minimal medium. * denotes that the growth rate changes significantly between two PQ concentrations (2-tailed Welch's *t* test, $P < 0.01$).

Computing and Explaining the Environment Dependency of ROS Tolerance. To investigate how environmental context affects ROS tolerance, we simulated growth under superoxide stress in 180 carbon sources (*SI Appendix*, Fig. S2). We then compared pairs of carbon sources in terms of the complexes that are most damaged by ROS. In particular, from simulations we predicted that a key bottleneck to growth on D-galactose under ROS stress is inactivation of shikimate kinase II, AroL (Fig. 2*D*). In contrast, AroL was predicted to not be a direct bottleneck to growth on glycolate (Fig. 2*D*). To validate this prediction, we measured growth of *E. coli* MG1655 on these two carbon sources in 0 to 0.6 μM paraquat (PQ). PQ is a divalent cation that is taken up opportunistically, typically by polyamine transmembrane transporters, and then undergoes reduction and autoxidation cycles catalyzed by any of three *E. coli* PQ diaphorases to generate superoxide (28). To directly test whether AroL is a bottleneck, we also supplemented the cultures with 50 μM shikimate. As predicted, shikimate did not alleviate PQ-induced growth defects during growth on glycolate (Fig. 2*E*). Meanwhile, shikimate alleviated growth defects by PQ during growth on D-galactose (Fig. 2*F*). These results confirm that OxidizeME is able to accurately predict ROS-induced amino acid auxotrophies in different environmental contexts. This predictive capability is rooted in its ability to compute molecular and macromolecular mechanisms.

We then used OxidizeME to explain why growth on glycolate and galactose exhibited different ROS tolerances. First, ROS stress globally increases redox balancing and energy production requirements to counter the lowered metabolic and protein expression efficiencies resulting from metalloprotein damage. Thus, the difference in *E. coli*'s capacity to replenish these metabolic capacities under different carbon sources can explain differences in ROS sensitivity.

During growth on D-galactose, the primary source of NADPH was the oxidative pentose phosphate pathway (Gnd and Zwf), with and without ROS stress. Under ROS stress with D-galactose as the carbon source, simulations indicated increased methylenetetrahydrofolate dehydrogenase (FolD) activity to supplement NADPH production by the PPP (pentose phosphate pathway), although PPP was still the major source of NADPH. Meanwhile, NADH production relied greatly on the glycine cleavage system with ROS, whereas glyceraldehyde-3-phosphate dehydrogenase was the primary source of NADH without ROS. The increase in FolD and glycine cleavage

system fluxes to replenish NADPH and NADH both increased the requirement for tetrahydrofolate and its derivatives, which created a new metabolic bottleneck under ROS stress. In contrast, with glycolate as the carbon source, optimal NADPH production was predicted to switch from the TCA cycle (no ROS) to malic enzyme (with ROS). Thus, the difference between ROS tolerance capacities for galactose and glycolate as carbon sources can be explained by flexible NADPH production during growth on glycolate vs. rigid NADPH production during growth on galactose.

OxidizeME Delineates Stress-Specific Differential Gene Expression from Global Expression Changes. Next, we assessed the systemic response of *E. coli* to ROS stress. We measured the transcriptome of *E. coli* under superoxide stress using PQ treatment and identified 914 differentially expressed genes (DEGs), of which 501 were accounted for in OxidizeME (Fig. 3 and *SI Appendix*, Fig. S3). In particular, 87 genes were up-regulated. Using OxidizeME, we determined that these 87 genes were more likely activated due to damage that is specific to iron metalloproteins than to any other protein ($P < 0.001$). Furthermore, of the DEGs that were correctly predicted, a large fraction (84%) of the repressed genes changed due to decreased growth rate from PQ treatment, while 95% of the activated genes were specific responses to stress (Fig. 3). Gene expression is expected to respond to ROS stress directly—e.g., by up-regulating ROS detoxification genes—and indirectly—in response to decreased metabolic rates caused by ROS damage. The responses we identified as being specific to ROS, not to growth rate, spanned eight cellular processes (Fig. 3): ROS detoxification, central metabolism, anaerobic respiration, amino acid biosynthesis, cofactor synthesis and repair, translation, iron homeostasis, and transcriptional regulation by the *rpoS* sigma factor.

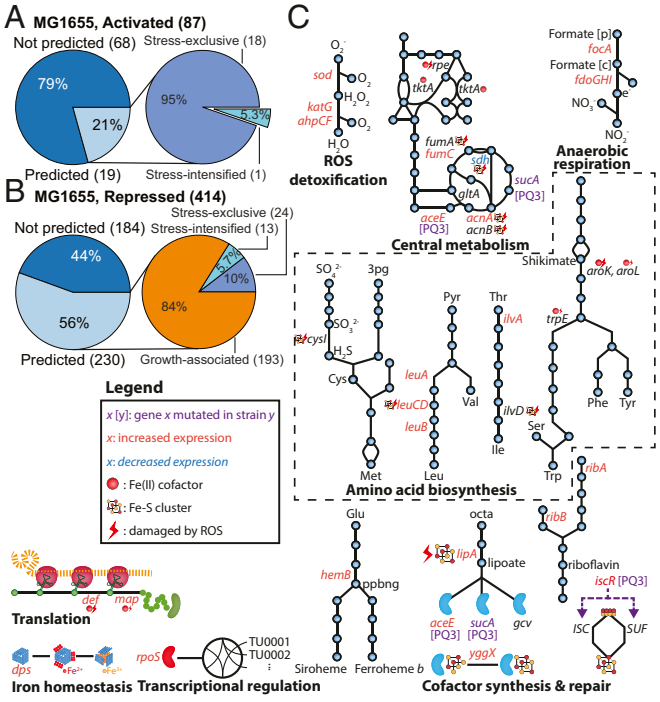

Fig. 3. Validation of the consequences and responses to ROS stress. (*A* and *B*) DEGs ($|\log_2(\text{fold change})| > 0.9$, FDR [false discovery rate] < 0.01) that are activated (*A*) and repressed (*B*). Correctly predicted DEGs are distinguished from global growth-associated regulation using OxidizeME. (*C*) Cellular processes involved in a systemic response to iron metalloprotein damage by ROS.

ROS-evolved cells deregulate Fe–S cluster biosynthesis. *E. coli* possesses two alternative systems to synthesize Fe–S clusters: ISC (iron–sulfur cluster) and SUF (sulfur assimilation). Each system can synthesize Fe–S clusters in the absence of the other (29). While ISC is predominant under normal growth conditions, SUF is activated and can become the primary system under oxidative or iron limitation stress (4, 30). One reason for this switch to SUF is that ROS lowers the efficiency of ISC-based Fe–S assembly by increasing mismetallation of labile iron–sulfur clusters on the scaffold proteins IscU and SufA (31). In principle, switching from ISC to SUF is not the only mechanism for sustaining Fe–S assembly under ROS stress. For example, *Mycobacterium tuberculosis* possesses only the ISC operon, yet this pathogen is able to grow under oxidative stress including inside macrophages, presumably by up-regulating its ISC operon (32). A possible explanation is that *M. tuberculosis*'s ISC scaffold proteins are less sensitive to ROS than those in *E. coli* or are repaired. However, *E. coli* also possesses several putative Fe–S cluster repair genes, including *ygfZ* (33), *yggX* (15), and *ytfE* (16). Overall, gaps exist in our understanding of the cost–benefit tradeoffs between ISC and SUF under ROS stress. Here, we investigate this problem using OxidizeME and experimental validation.

First, we detected DEGs in wild-type *E. coli* MG1655 in response to 0.25 mM PQ, using RNA-Seq in glucose minimal medium. We detected repression of *iscRSUA* (mean $\log_2$ (fold change) $= -1.53$, FDR-adjusted $P < 0.001$). We then repeated this experiment with an *E. coli* strain (called BOP1000) that had been evolved to grow rapidly on glucose (34). As with MG1655, strain BOP1000 repressed *iscRSUA* (mean $\log_2$ (fold change) $= -1.32$, FDR-adjusted $P < 0.053$) (Dataset S3).

Finally, we obtained a laboratory-evolved strain of *E. coli* (called PQ3), which was evolved to grow on 0.8 mM PQ (*SI Appendix*, *SI Materials and Methods*). The starting strain for PQ3 is the glucose-evolved BOP1000. We cultured PQ3 in 0.2 and 0.6 mM PQ and identified DEGs using RNA-Seq. Under 0.6 mM PQ, strain PQ3 down-regulated the *sufABCDSE* transcription unit (mean $\log_2$ (fold change) $= -2.01$, FDR-adjusted $P < 0.034$) (Dataset S3). Furthermore, under 0.2 mM PQ, strain PQ3 maintained higher expression of ISC compared with the preevolved BOP1000 strain. Specifically, we observed higher expression of the transcription units *iscRSUA* (mean $\log_2$ (fold change) $=3.47$, FDR-adjusted $P < 0.001$) and *hscBA-fdx-iscX* (mean $\log_2$ (fold change) $=1.99$, FDR-adjusted $P < 0.001$) (Dataset S3).

The contrasting transcriptomic response of the PQ-evolved strain from those of the glucose-evolved and wild-type strains prompted us to investigate genetic and systems-level mechanisms for ROS adaptation.

Genetic and Systems-Level Mechanisms of Optimal Fe–S Cluster Biosynthesis. The genetic basis for the PQ-evolved response of ISC and SUF was a mutation in *iscR*. IscR regulates the transcription of both ISC and SUF based on coordination of 2Fe–2S at its Cys92, Cys98, and Cys104 residues (29, 35). The evolved strain had mutation C104S in *iscR*. This mutation may hinder IscR's ability to incorporate 2Fe–2S and to regulate expression of the ISC and SUF systems under ROS stress (35).

We then investigated why increasing ISC and repressing SUF improve fitness under sustained ROS stress. Clearly, we expect a tradeoff between the rate of Fe–S inactivation at IscU and the fitness advantage of using SUF. Indeed, simulations show that below a threshold rate of Fe–S inactivation at IscU ($\sim 0.78\ s^{-1}$), sulfur transfer during Fe–S assembly occurs almost exclusively by IscS rather than by SufSE (*SI Appendix*, Fig. S4). Interestingly, IscU expression is predicted to increase proportionally to Fe–S inactivation rate up until the threshold, indicating an initial

compensatory response to lowered Fe–S assembly efficiency at IscU. However, above the threshold, expression of IscU and IscS drops sharply, while SufSE and SufBCD expression increases. One reason for the fitness advantage of ISC over SUF is the cost of protein expression for each system. Considering just the sulfur transfer and scaffold complexes, IscS and IscU require 118 kDa of protein translated, while SufSE and $SufBC_2D$ require 227 kDa—93% more than ISC.

Thus, increased ISC expression suggests that strain PQ3 may experience lowered Fe–S inactivation at IscU. To investigate this possibility, recall that *E. coli* possesses several genes associated with repair or oxidation resistance of Fe–S clusters, including *ygfZ* (33), *yggX* (15), and *ytfE* (16). RNA-Seq (Dataset S3) showed that none of these genes were differentially expressed by strain PQ3 in response to PQ. There was also no difference in expression level compared with strain BOP1000 under PQ treatment. However, DNA-Seq revealed a mutation (T108P) in *ygfZ*, a gene thought to contribute to Fe–S cluster synthesis or repair (33). Alternatively, *ygfZ* may directly degrade PQ, since it was shown to degrade plumbagin, another redox cycling compound (36). Either adaptive function would be consistent with lessened damage to Fe–S clusters overall; however, it is unclear whether protecting Fe–S clusters at IscU is sufficient to reproduce the observed increase of ISC expression (and repression of SUF).

We thus performed simulations where we set the damage rate to Fe–S clusters at IscU to zero and kept damage processes for all other iron and Fe–S cluster-containing complexes. We then simulated growth of *E. coli* under basal (0.2 nM) and high (2 nM) intracellular concentrations of superoxide and identified in silico DEGs. Simulated DEGs were consistent with RNA-Seq of PQ3: *hscBA-fdx-iscX* and *iscRSUA* operons were up-regulated, and *sufABCDSE* was repressed (Dataset S4). This result indicates that protecting Fe–S clusters at IscU is sufficient to make ISC more favorable than SUF under ROS stress. The PQ-evolved strain potentially achieves this protection through *ygfZ* and in turn switches to the more advantageous ISC by mutation of *iscR*.

Discussion

The use of iron–sulfur clusters and transition metals to catalyze biological processes can be traced back to the last universal common ancestor (37) and ROS stress has a profound impact on all aerobic life forms. OxidizeME advances our understanding of stress-response mechanisms by providing a genome-wide description of metabolism, protein expression, prosthetic group engraftment, and ROS protecting mechanisms that collectively account for up to 85% of the proteome by mass.

We used OxidizeME to predict and explain four cellular responses of *E. coli* to ROS. 1) Our model correctly predicted amino acid auxotrophy under ROS stress and traced the molecular mechanisms to the correct target enzymes for aromatic and branched-chain amino acids. 2) We used OxidizeME to identify a pair of carbon sources (glycolate and galactose) predicted to display differential ROS sensitivity, out of 180 possible sources. By tracing the metalloprotein targets of ROS, we designed shikimate supplementation experiments predicted to restore growth in galactose but not in glycolate under ROS stress. Experiments confirmed our predictions. Furthermore, our model suggested that ROS sensitivity increased when *E. coli* was grown on galactose due to suboptimal NAD(P)H production that relied heavily on folate metabolism. Drugs that target folate metabolism are available (e.g., trimethoprim) (38), and future studies may explore interventions that combine ROS, disruption of folate metabolism, and specific nutrient perturbations. 3) We delineated 56 ROS-specific DEGs from global expression change resulting from decreased growth rate under ROS stress. (*iv*) OxidizeME provided an explanation for a nonintuitive cellular behavior in ROS-evolved strains: An inverted preference for using ISC over SUF under ROS stress, contrasting with ISC repression in both wild-type and glucose-evolved *E. coli*. Our model showed that ISC is preferable over SUF under ROS stress when the rate of Fe–S cluster inactivation at IscU scaffolds remains below a threshold. Below that threshold, ISC is activated proportionally with ROS stress, and above the threshold the switch from ISC to SUF occurs. A mutation in *ygfZ* supported our hypothesis that Fe–S inactivation at IscU is possibly lowered, while a mutation in *iscR* explained how the ROS-evolved strain deregulated ISC and SUF.

In this work, we extended the ME modeling framework (9, 13, 39) by accounting for chemical (oxidative) stress to macromolecules. Previously, FoldME (40) enabled simulation of thermal stress response. In this way, ME models can be extended to model major physicochemical stresses. Microbial stress response is thought to play an important role in infectious disease (41, 42), and systems-level reconstructions of stress response can facilitate model-driven discovery of antimicrobials. For example, to kill pathogens, macrophages use ROS (oxidative burst), acidification, and accumulation of toxic metals including zinc and copper (43). We showed that OxidizeME computes fitness defects caused by ROS and disruption of metal ion homeostasis. Therefore, our model and its extensions can be valuable for investigating host–pathogen interactions. Fundamentally, the ability to quantitatively and mechanistically describe responses to the damage of ancient conserved molecular targets by ROS and other physicochemical factors has broad implications for organisms across the tree of life.

Materials and Methods

Computing with OxidizeME. We compute solutions to Eq. **6** using QuadMINOS (44) via the solveME Python module (10).

Differentiating Stress-Specific from Growth-Associated Responses. Using OxidizeME, we compute growth rate at various intracellular superoxide concentrations. At these growth rates, we compute the transcriptome of the basic ME model (without stress response) to identify DEGs that are associated with lowered growth. DEGs that are correctly predicted by OxidizeME but not by ME are stress associated. DEGs that are correctly predicted by ME and do not considerably change expression in OxidizeME are growth associated.

Model-Computed Differentially Expressed Genes. We use OxidizeME to classify genes as activated, repressed, or unchanged in expression in response to ROS. We compute the change in transcription rates of all transcription units in the model for intracellular superoxide concentrations ranging from 0.2 to 2 nmol, which is ∼10 to 100 times the concentration under aerobic growth without PQ. We then use the average transcription rate changes. Because certain genes change expression nonlinearly with superoxide concentration, including an inverse response, and because the transcription rate change depends on the reference state simulation, we also compute the Spearman rank correlation of transcription rate with superoxide concentration. Thus, if a gene has a lower relative rate than the reference but its rate is positively and significantly ($P < 0.05$) correlated with superoxide, we use this Spearman rank to predict expression change. We then classify genes as activated or repressed based on a threshold transcription rate change, which we vary and investigate using a precision-recall curve. The best classification is chosen using the threshold that maximizes $F = 2 \cdot \text{precision} \cdot \text{recall}/(\text{precision} + \text{recall})$ (*SI Appendix*, Fig. S3).

Randomly Sampling the Scope of Metalloprotein Damage. To investigate whether the proteins damaged by ROS are limited to the 43 iron metalloproteins, we simulated response to ROS for 1,000 models. In each model, we inactivated a random set of 43 enzymes. Of the 1,000 random models, 26 (2.6%) overlapped with measured down-regulated genes as well as or better than our model, while none overlapped with up-regulated genes as well as our model. Therefore, ROS is significantly more likely to damage

the 43 iron metalloproteins studied here than any other set of 43 proteins randomly chosen from the 1,582 proteins in OxidizeME.

Data Availability. Code to build and use OxidizeME is available at https://github.com/SBRG/oxidizeme (45). Mutations for strain PQ3 are reported in ALEdb (46): https://aledb.org (Project ID OxidizeME) (47).

ACKNOWLEDGMENTS. This work was supported by the National Institute of General Medical Sciences of the National Institutes of Health Grants U01GM12098 and R01GM057089 and Novo Nordisk Foundation Grant NNF10CC1016517. This research used resources of the National Energy Research Scientific Computing Center, a Department of Energy (DOE) Office of Science User Facility supported by the Office of Science of the US DOE under Contract DE-AC02-05CH11231.

1. S. A. Crowe *et al.*, Atmospheric oxygenation three billion years ago. *Nature* **501**, 535–538 (2013).
2. M. P. Brynildsen, J. A. Winkler, C. S. Spina, I. C. MacDonald, J. J. Collins, Potentiating antibacterial activity by predictably enhancing endogenous microbial ROS production. *Nat. Biotechnol.* **31**, 160–165 (2013).
3. J. M. Monk *et al.*, iML1515, a knowledgebase that computes Escherichia coli traits. *Nat. Biotechnol.* **35**, 904 (2017).
4. J. A. Imlay, The molecular mechanisms and physiological consequences of oxidative stress: Lessons from a model bacterium. *Nat. Rev. Microbiol.* **11**, 443–454 (2013).
5. J. A. Imlay, Iron-sulphur clusters and the problem with oxygen. *Mol. Microbiol.* **59**, 1073–1082 (2006).
6. J. A. Imlay, Where in the world do bacteria experience oxidative stress? *Environ. Microbiol.* **21**, 521–530 (2019).
7. M. A. Bringer, N. Barnich, A. L. Glasser, O. Bardot, A. Darfeuille-Michaud, Htra stress protein is involved in intramacrophagic replication of adherent and invasive Escherichia coli strain lf82 isolated from a patient with Crohn's disease. *Infect. Immun.* **73**, 712–721 (2005).
8. J. A. Imlay, R. Sethu, S. K. Rohaun, Evolutionary adaptations that enable enzymes to tolerate oxidative stress. *Free Radic. Bio. Med.*, 10.1016/j.freeradbiomed.2019.01.048 (2019).
9. L. Yang, J. T. Yurkovich, Z. A. King, B. O. Palsson, Modeling the multi-scale mechanisms of macromolecular resource allocation. *Curr. Opin. Microbiol.* **45**, 8–15 (2018).
10. L. Yang *et al.*, solveME: Fast and reliable solution of nonlinear ME models. *BMC Bioinform.* **17**, 391 (2016).
11. C. J. Lloyd *et al.*, Cobrame: A computational framework for genome-scale models of metabolism and gene expression. *PLoS Comput. Biol.* **14**, e1006302 (2018).
12. I. Thiele, N. Jamshidi, R. M. Fleming, B. Ø. Palsson, Genome-scale reconstruction of Escherichia coli's transcriptional and translational machinery: A knowledge base, its mathematical formulation, and its functional characterization. *PLoS Comput. Biol.* **5**, e1000312 (2009).
13. I. Thiele *et al.*, Multiscale modeling of metabolism and macromolecular synthesis in *E. coli* and its application to the evolution of codon usage. *PLoS One* **7**, e45635 (2012).
14. E. J. O'Brien, J. A. Lerman, R. L. Chang, D. R. Hyduke, B. O. Palsson, Genome-scale models of metabolism and gene expression extend and refine growth phenotype prediction. *Mol. Syst. Biol.* **9**, 693 (2013).
15. P. J. Pomposiello, A. Koutsolioutsou, D. Carrasco, B. Demple, Soxrs-regulated expression and genetic analysis of the yggx gene of Escherichia coli. *J. Bacteriol.* **185**, 6624–6632 (2003).
16. L. S. Nobre *et al.*, Escherichia coli ric is able to donate iron to iron-sulfur clusters. *PLoS One* **9**, e95222 (2014).
17. J. A. Imlay, The mismetallation of enzymes during oxidative stress. *J. Biol. Chem.* **289**, 28121–28128 (2014).
18. J. M. Sobota, J. A. Imlay, Iron enzyme ribulose-5-phosphate 3-epimerase in Escherichia coli is rapidly damaged by hydrogen peroxide but can be protected by manganese. *Proc. Natl. Acad. Sci. U.S.A.* **108**, 5402–5407 (2011).
19. J. M. Sobota, M. Gu, J. A. Imlay, Intracellular hydrogen peroxide and superoxide poison 3-deoxy-d-arabinoheptulosonate 7-phosphate synthase, the first committed enzyme in the aromatic biosynthetic pathway of Escherichia coli. *J. Bacteriol.* **196**, 1980–1991 (2014).
20. A. Schmidt *et al.*, The quantitative and condition-dependent Escherichia coli proteome. *Nat. Biotechnol.* **34**, 104–110 (2016).
21. L. Macomber, J. A. Imlay, The iron-sulfur clusters of dehydratases are primary intracellular targets of copper toxicity. *Proc. Natl. Acad. Sci. U.S.A.* **106**, 8344–8349 (2009).
22. L. Benov, I. Fridovich, Why superoxide imposes an aromatic amino acid auxotrophy on Escherichia coli the transketolase connection. *J. Biol. Chem.* **274**, 4202–4206 (1999).
23. N. Pollak, C. Dölle, M. Ziegler, The power to reduce: Pyridine nucleotides–small molecules with a multitude of functions. *Biochem. J.* **402**, 205–218 (2007).
24. L. Benov, I. Fridovich, Superoxide imposes leakage of sulfite from Escherichia coli. *Arch. Biochem. Biophys.* **347**, 271–274 (1997).
25. K. R. Messner, J. A. Imlay, The identification of primary sites of superoxide and hydrogen peroxide formation in the aerobic respiratory chain and sulfite reductase complex of Escherichia coli. *J. Biol. Chem.* **274**, 10119–10128 (1999).
26. M. P. Thorgersen, D. M. Downs, Oxidative stress and disruption of labile iron generate specific auxotrophic requirements in Salmonella enterica. *Microbiology* **155**, 295–304 (2009).
27. L. Benov, N. M. Kredich, I. Fridovich, The mechanism of the auxotrophy for sulfur-containing amino acids imposed upon Escherichia coli by superoxide. *J. Biol. Chem.* **271**, 21037–21040 (1996).
28. S. I. Liochev, A. Hausladen, W. F. Beyer, I. Fridovich, NADPH: Ferredoxin oxidoreductase acts as a paraquat diaphorase and is a member of the soxrs regulon. *Proc. Natl. Acad. Sci. U.S.A.* **91**, 1328–1331 (1994).
29. E. L. Mettert, P. J. Kiley, Coordinate regulation of the SUF and ISC FE-S cluster biogenesis pathways by iscr is essential for viability of Escherichia coli. *J. Bacteriol.* **196**, 4315–4323 (2014).
30. B. Roche *et al.*, Reprint of: Iron/sulfur proteins biogenesis in prokaryotes: Formation, regulation and diversity. *Biochim. Biophys. Acta Bioenerg.* **1827**, 923–937 (2013).
31. C. Ranquet, S. Ollagnier-de Choudens, L. Loiseau, F. Barras, M. Fontecave, Cobalt stress in Escherichia coli the effect on the iron-sulfur proteins. *J. Biol. Chem.* **282**, 30442–30451 (2007).
32. M. Pandey, S. Talwar, S. Bose, A. K. Pandey, Iron homeostasis in mycobacterium tuberculosis is essential for persistence. *Sci. Rep.* **8**, 17359 (2018).
33. J. C. Waller *et al.*, A role for tetrahydrofolates in the metabolism of iron-sulfur clusters in all domains of life. *Proc. Natl. Acad. Sci. U.S.A.* **107**, 10412–10417 (2010).
34. R. A. LaCroix *et al.*, Use of adaptive laboratory evolution to discover key mutations enabling rapid growth of *Escherichia coli* K-12 MG1655 on glucose minimal medium. *Appl. Environ. Microbiol.* **81**, 17–30 (2015).
35. S. Rajagopalan *et al.*, Studies of iscr reveal a unique mechanism for metal-dependent regulation of DNA binding specificity. *Nat. Struct. Mol. Biol.* **20**, 740–747 (2013).
36. C. N. Lin *et al.*, A role of ygfz in the Escherichia coli response to plumbagin challenge. *J. Biomed. Sci.* **17**, 84 (2010).
37. M. C. Weiss *et al.*, The physiology and habitat of the last universal common ancestor. *Nat. Microbiol.* **1**, 16116 (2016).
38. Y. K. Kwon *et al.*, A domino effect in antifolate drug action in Escherichia coli. *Nat. Chem. Biol.* **4**, 602–608 (2008).
39. L. Yang, A. Ebrahim, C. J. Lloyd, M. A. Saunders, B. O. Palsson, Dynamicme: Dynamic simulation and refinement of integrated models of metabolism and protein expression. *BMC Syst. Biol.* **13**, 2 (2019).
40. K. Chen *et al.*, Thermosensitivity of growth is determined by chaperone-mediated proteome reallocation. *Proc. Natl. Acad. Sci. U.S.A.* **114**, 11548–11553 (2017).
41. J. L. Radzikowski *et al.*, Bacterial persistence is an active σ s stress response to metabolic flux limitation. *Mol. Syst. Biol.* **12**, 882 (2016).
42. J. L. Radzikowski, H. Schramke, M. Heinemann, Bacterial persistence from a system-level perspective. *Curr. Opin. Biotech.* **46**, 98–105 (2017).
43. T. Soldati, O. Neyrolles, Mycobacteria and the intraphagosomal environment: Take it with a pinch of salt (s)! *Traffic* **13**, 1042–1052 (2012).
44. D. Ma *et al.*, Reliable and efficient solution of genome-scale models of metabolism and macromolecular expression. *Sci. Rep.* **7**, 40863 (2017).
45. L. Yang, Data from "OxidizeME model and notebooks." GitHub. https://github.com/SBRG/oxidizeme. Deposited 13 September 2018.
46. P. V. Phaneuf, D. Gosting, B. O. Palsson, A. M. Feist, Aledb 1.0: A database of mutations from adaptive laboratory evolution experimentation. *Nucleic Acids Res.* **47**, D1164–D1171 (2018).
47. P. V. Phaneuf, Project: OxidizeME. ALEdb. https://aledb.org/ale/project/23/. Deposited 6 June 2019.